Vibration enhanced cell growth induced by surface acoustic waves as in vitro wound-healing model

Manuel S. Brugger[a,b], Kathrin Baumgartner[a,c], Sophie C. F. Mauritz[a], Stefan C. Gerlach[a,d], Florian Röder[a], Christine Schlosser[e], Regina Fluhrer[e,f], Achim Wixforth[a,g], and Christoph Westerhausen[a,g,h,1]

[a]Experimental Physics I, Institute of Physics, University of Augsburg, 86159 Augsburg, Germany; [b]Stiftung der Deutschen Wirtschaft gGmbH, 10178 Berlin, Germany; [c]Studienstiftung des deutschen Volkes e.V., 53175 Bonn, Germany; [d]Hans-Seidel-Stiftung e.V., 80636 Munich, Germany; [e]Biochemistry and Molecular Biology, Institute of Theoretical Medicine, University of Augsburg, 86159 Augsburg, Germany; [f]German Center for Neurodegenerative Diseases (DZNE) e.V., 81377 Munich, Germany; [g]Center for NanoScience, 80799 Munich, Germany; and [h]Physiology, Institute of Theoretical Medicine, University of Augsburg, 86159 Augsburg, Germany

Edited by Tony Jun Huang, Duke University, Durham, NC, and accepted by Editorial Board Member Tony Hunter November 2, 2020 (received for review March 23, 2020)

We report on in vitro wound-healing and cell-growth studies under the influence of radio-frequency (rf) cell stimuli. These stimuli are supplied either by piezoactive surface acoustic waves (SAWs) or by microelectrode-generated electric fields, both at frequencies around 100 MHz. Employing live-cell imaging, we studied the time- and power-dependent healing of artificial wounds on a piezoelectric chip for different cell lines. If the cell stimulation is mediated by piezomechanical SAWs, we observe a pronounced, significant maximum of the cell-growth rate at a specific SAW amplitude, resulting in an increase of the wound-healing speed of up to 135 ± 85% as compared to an internal reference. In contrast, cells being stimulated only by electrical fields of the same magnitude as the ones exposed to SAWs exhibit no significant effect. In this study, we investigate this effect for different wavelengths, amplitude modulation of the applied electrical rf signal, and different wave modes. Furthermore, to obtain insight into the biological response to the stimulus, we also determined both the cell-proliferation rate and the cellular stress levels. While the proliferation rate is significantly increased for a wide power range, cell stress remains low and within the normal range. Our findings demonstrate that SAW-based vibrational cell stimulation bears the potential for an alternative method to conventional ultrasound treatment, overcoming some of its limitations.

surface acoustic waves | vibration | cell migration | stimulation | cell growth

Currently, improving and acceleration of wound-healing is of highest interest in medical science. Reports of "smart" wound-healing techniques range from on-demand emission of inflammatory-inhibiting materials (1) to increased cell growth by releasing growth factors upon cell-induced traction forces (2). There also have been reports on techniques including active electrical and mechanical cell stimulation, e.g., by using sound-waves. Already in the 1960s, Knoch (3) and Klug and coworkers (4) proposed the use of therapeutic ultrasound (US). Since then, it has been shown that US can in fact improve the regeneration and healing rate of soft and hard tissue up to 40% (5–7) for spatially distributed intensities between I_{US} = 30 mW/cm^2 and I_{US} = 500 mW/cm^2 (8, 9). Furthermore, the potential of US treatment to stimulate the spleen in order to treat inflammatory diseases has been recently demonstrated (10). Despite the obviously beneficial effects of therapeutic US, the application of the technique is still subject to restrictions. It turns out, for example, that the beneficial effects of US undergo a turnaround, leading to a suppressed fracture-healing if the US intensity applied is higher than I_{US} = 1 W/cm^2 (11). In this context, it has been shown that US application may induce a temperature rise in tissue of about 0.86 K/min at a power of 1 W/cm^2 and a frequency of 1 MHz (12), limiting the US therapy to short pulses and low intensities of about I = 30 mW/cm^2 (13). Moreover, high costs and the requirement of medical assistance during US exposure impede a long-term treatment and limit the application to single sessions. As an answer to these limitations, we recently proposed an approach employing surface acoustic waves (SAWs) for tissue-healing and -recovery treatment to overcome some disadvantages of the US-based methods (14). In recent years, SAWs can be found as mass products in, e.g., filters and radio frequency (rf)-signal processing devices in mobile phones and high-frequency applications but also for the active acoustic manipulation in microfluidic applications. Based on the effect of acoustic streaming (15), SAWs have recently become a quite unique tool in biomedical applications for cell manipulation (16), deadhesion under flow (17), or on-demand patterning (18). Moreover, first results show that SAW-based biochips can yield tailored standing wave-body force fields, which bear the fascinating potential to create a well-defined neural network on a chip (19). In a recent report on SAW-assisted in vitro wound-healing, we were able to demonstrate positive stimulation of cell growth up to 15.2 ± 1.7%. After carefully excluding parasitic temperature-, ballistic-, or nutrient-induced stimulation effects, we were able to narrow down the beneficial SAW-induced mechanisms to the mechanical and electrical component of the SAW. Our findings were later confirmed and supported by

Significance

Ultrasonic pressure fields have been proven to be beneficial for cell growth in vitro and in patients. However, conventional therapeutic-ultrasound treatment is subjected to limitations such as time restriction, external application, or energy loss. The application of surface acoustic waves (SAWs) can help to overcome some drawbacks. To understand the underlying mechanism, the adjusting parameters of SAWs and the intracellular response to the stimulation are evaluated. We identified a dependence of cell growth on SAW intensity and the presence of a vertical substrate deflection. While the cellular stress (reactive oxygen species) remains in the normal range, both cell migration and proliferation are increased. Due to the experimental design, the effect of enhanced cell growth is dominated by increased cell migration.

Author contributions: M.S.B., R.F., A.W., and C.W. designed research; M.S.B., K.B., S.C.F.M., S.C.G., F.R., C.S., R.F., and C.W. performed research; M.S.B., C.S., R.F., and C.W. contributed new reagents/analytic tools; M.S.B., K.B., S.C.F.M., S.C.G., F.R., C.S., R.F., and C.W. analyzed data; and M.S.B. and C.W. wrote the paper.

The authors declare no competing interest.

This article is a PNAS Direct Submission. T.J.H. is a guest editor invited by the Editorial Board.

[1]To whom correspondence may be addressed. Email: christoph.westerhausen@gmail.com.

This article contains supporting information online at https://www.pnas.org/lookup/suppl/doi:10.1073/pnas.2005203117/-/DCSupplemental.

First published November 30, 2020.

Greco et al., who investigated the impact of SAWs on cell proliferation (20).

In this article, we continue on the impact of SAW stimulation on cell growth, narrow down the stimulation mechanism, identify the most relevant adjusting parameters, and provide insights into the intracellular reactions induced by SAWs. Moreover, we also address the question of whether the observed phenomenon is due to cell migration or proliferation.

Methods and Materials

If not stated otherwise, in vitro wound-healing assays were performed while measuring cellular parameters for three cell lines: Madine–Darby canine kidney (MDCK-II), human osteosarcoma sarcoma osteogenic (SaOs-2), and human embryonic kidney (T-REx-293). For detailed information, see *SI Appendix*.

The Experimental Setup. A SAW chip is a piezoelectric chip with micron-sized metal electrodes, so-called interdigital transducers (IDTs), consisting of two multifinger electrodes (21). An rf signal of power P_{IN} and frequency f_{res} is converted into an acoustic wave with a width of the transducer and a wavelength of λ_{SAW}. Dependent on the substrate, cut, and transducer design, the wave is either a Rayleigh SAW for $LiNbO_3$ rotated around the *x* axis by 128° (128° rotated [rot] *y*-cut) or a Love wave (LW) for $LiTaO_3$ (40° rot *xy*-cut) (22). To ensure biocompatibility and to protect the electrodes, the whole chip except for the contact pads is covered with a SiO_2 layer.

Due to the IDTs' bidirectionality (3 dB) as well as based on years of experience with SAW with various other, small insertion-loss mechanisms, we conservatively estimated P_{SAW} of the propagating wave as $P_{SAW} \sim 1/4\ P_{IN}$. The SAW causes acoustic streaming (23) with a 1/*e* decay length of the SAW-intensity in the propagation direction of $l_{op}^{Calc}{}_{x} = 12.5\lambda_{SAW} = 331\ \mu m$ (24). Considering $l_{op}^{Calc}{}_{x}$, P_{SAW}, and *W*, the SAW intensity, I_{SAW}, acting upon the cells is approximately (24):

$$I_{SAW} = P_{SAW}\frac{\left(1-\frac{1}{e}\right)}{W\ l_{op}^{Calc}{}_{x}} \approx 80\ \frac{mW}{\frac{C}{cm}}$$

for $P_{IN} = 1$ mW and

$$I_{SAW} \approx 1\ \frac{W}{\frac{C}{cm}}$$

for $P_{IN} = 13.6$ mW.

The SAW chip was mounted on a sample holder (Fig. 1 *A*, *a-2*). A polydimethylsiloxane chamber ($V = 3$ mL) (Sylgard 184 Silicone Elastomer; Dow Corning) was placed on top of the SAW chip (Fig. 1 *A*, *a-1*). The culture insert (CI) (width, 500 ± 50 μm; Ibidi GmbH) was placed with its gap oriented parallel to and about $d = 50$ μm away from the IDT (Fig. 1 *A*, *a-3*); 80,000 cells were seeded into each chamber and cultivated to reach confluency. After removal of the CI, the cell migration into the cell-free area was recorded in phase-contrast images every 5 min with a 10× objective. The SAW-chips were connected to an rf generator (SML 01; Rhode & Schwarz) with an amplifier (gain, 30 dB; AMP590033H-T; Becker Nachrichtentechnik GmbH).

Characterization of the Resulting Flow Field. We determined the effective flow field 25 μm above the surface using scanning-particle image velocimetry (sPIV), as reported earlier (25), by scanning an area larger than a single field of view and combining the multiple microparticle image-velocimetry measurements to a single velocity field.

Measuring Intracellular Parameters. To understand the cellular response and the biochemical processes, we determined the production of reactive oxygen species (ROS), the proliferation rate, and their internal and external reference following standard protocols (see *SI Appendix* for details).

Data Analysis.

Wound-healing assays. Fig. 1*B* shows a chronological sequence of a typical experiment with MDCK-II cells at different time points. The cell fronts continuously invade the red-labeled cell-free area. Based on previous experiments, we know that the width of the sound path is strictly limited to the size of the aperture (26). Therefore, only cells in front and rear of the aperture are directly stimulated by SAWs. The cell-free area in this region is called "aperture" in the following. As shown in Fig. 1 *C*, *Inset*, the internal references indicated in green and blue are located next to the wiring. At these positions, there is sufficient distance that the SAW does not interact with the cells. However, cells grow under identical conditions (i.e., nutrient supply, temperature, cell density, cell cycle, viability, etc.) as in front of the aperture.

The surface area migration rate (A_{mig}) describes the speed of cell migration and growth into the free space. The cell-free area is determined for every region of interest in $\Delta t = 1.25$-h intervals and plotted as a function of the time in Fig. 1*C* normalized to $F(0)$ and approximated by a linear fit. To exclude artifacts, like delay time due to cellular polarization in the beginning or nonuniform surface-coverage before reaching confluency, only values in the interval $0.8 < F(t) < 0.2$ are fitted linearly (27), resulting in A_{mig} with the unit area loss in percent per hour. To compare the results and to avoid culture-dependent influences, the aperture $A_{mig,\ aperture}$ is divided by the mean of the internal references $A_{mig,\ int.\ ref.}$ and defined as stimulation efficacy $E = A_{mig,\ aperture}/A_{mig,\ int.\ ref.}$ (Fig. 2*D*). For each power, four separate experiments are performed if not indicated otherwise.

Superimposed composition to the complete sequence of one sample allows identification of the cell migration over time in one color-coded image, as shown in Fig. 1*D*. Dependent on the elapsed time, the rainbow-color changes from purple to deep red (early coverage results in blue tones). An exemplary development of a superimposed image as a result of the temporal evolution of the cell migration can be found in Movie S3. To maintain a high-quality content of the data, the cell layer in the analyzed region must meet specific demands like confluency, cell density, and viability. As exemplarily shown in Fig. 1*D-3*, the right part of the cell layer was not completely confluent as compared to the one in Fig. 1 *D-1* and *D-2*. Raw data to these superimposed images can be found in Movie S2 (Fig. 1*D-1*) and Movie S3 (Fig. 1*D-2*). Therefore, only the left part was considered for the internal reference. However, this concerns only a small fraction of all samples.

The variation of the speed of coverage of the cell-free area along this artificial wound is studied in more detail in *SI Appendix*.

Fluorescence images. To evaluate fluorescence images, the data were analyzed using a self-developed software in MATLAB (MathWorks), as described in detail in *SI Appendix*.

Results and Discussion

A previous study showed successful stimulation of SaOs-2 cells for continuous stimulation with Rayleigh modes of wavelength $\lambda = 25$ μm in the power range of $P_{IN} = 4$ to 8 mW. The structure of the study presented here is as follows. Firstly, based on our previously reported findings, we vary the wavelength, wave mode, and the duty cycle of the stimulation to identify the most relevant SAW parameters to answer the following questions: 1) Does an increase of λ further enhance the effect? 2) Do shear waves also result in a significant effect? 3) Do pulsed Rayleigh waves (RWs) also result in enhanced wound-healing on a chip?

Secondly, we can positively state that the effect is conserved for other cell lines and collective cell migration. We elucidate in depth the dependence of the effect on the applied power level. Thirdly, to further identify the intracellular response, we quantify ROS. Finally, we answer the question of whether the increased wound-healing is due to enhanced cell migration or proliferation.

Identifying the Most Relevant SAW Parameters for Cell Stimulation. After the successful verification of the positive impact of SAWs on cell growth in previous studies (14, 20), we now elucidate adjustment parameters of the observed effect. In the first approach, we identified an increased cell growth of SaOs-2 cells up to 15.2 ± 1.7% using RWs at $\lambda_{SAW} = 25$ μm and $P_{IN} = 4$ mW (14). The high degree of variability of SAW excitation raises the question of which parameters might have the largest influence on cell stimulation. The physical properties of the SAW depend on various parameters of the chip and the SAW-generating system. Here, we vary wave mode, wavelength, magnitude, and shape or envelope of the SAW amplitude. However, due to the immense width of the multidimensional parameter space, a systematic variation in this study primarily covers the SAW power level and thus amplitude. First, the employed piezoelectric substrate material and the direction of SAW propagation with respect to the crystal axis defines the type and mode of the SAW. While RWs are excited on $LiNbO_3$ 128° rot *y*-cut in the main direction, LWs

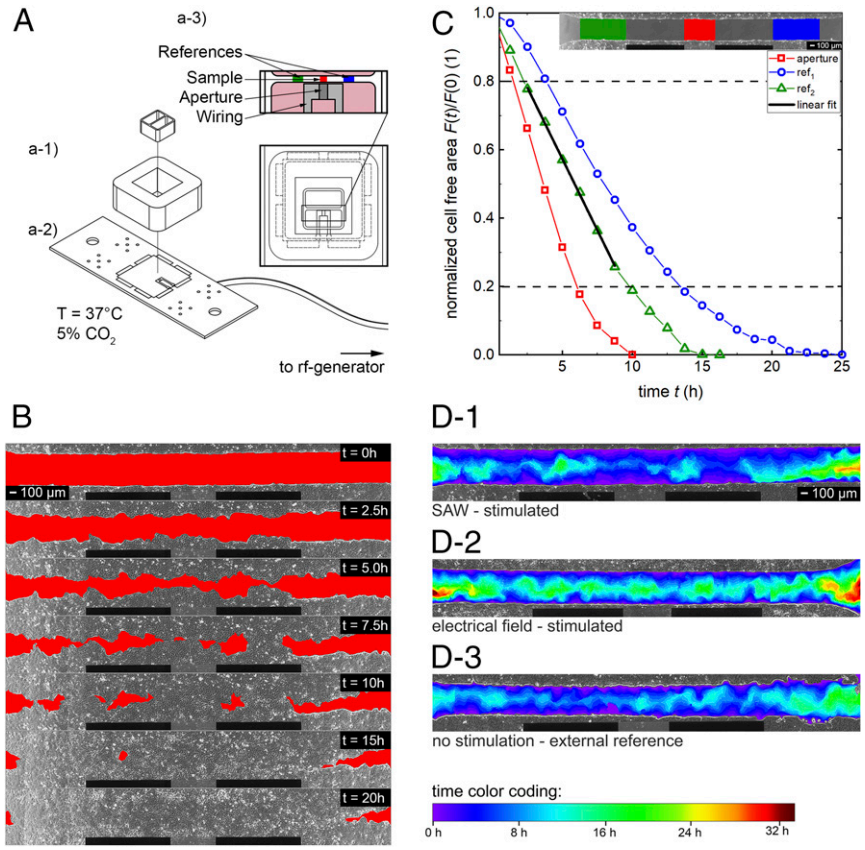

Fig. 1. Sketch of the experimental setup and concept of the data analysis. (*A*) Technical drawing of the setup. A culture insert was used to produce a standardized artificial wound in a confluent cell layer (pink) of MDCK-II cells in front of the IDT aperture. (*B*) Time-sequenced images of the progressive cell migration of MDCK-II cells into the cell-free area (red). (*C*) Time-dependent shrinkage of the normalized cell-free area in the regions of interest (red: stimulated section; green/blue: internal reference). The section between $0.8 < F(t)/F(0) < 0.2$ is approximated by a linear fit. The slope gives the surface area migration rate (A_{mig}). (*D*) Superimposed snapshots of the cell fronts of single experiments at different time steps with a time-dependent color-coded migration progress. (*D-1* and *D-2*) Analyzable samples. (*D-3*) Cell-layer quality of the right area does not meet the requirements.

can be generated on $LiTaO_3$ 40° rot *xy*-cut (22). In contrast to the RW, the excited LWs exhibit no surface deformation in the *z* direction but are horizontally polarized waves. Second, the propagation direction, wavelength, and width of the sound path of the excited SAWs are defined by the geometry and layout of the IDT being processed on the substrate surface. Third, by varying the rf-signal amplitude as a function of time, an amplitude modulated (AM) SAW of variable intensity can be generated.

Wavelength. In Fig. 2, the results of experiments with different SAW characteristics are shown. Changing the IDT periodicity from $\lambda_1 = 25$ µm to $\lambda_2 = 50$ µm leads to an accordingly reduced resonance frequency. In Fig. 2*A*, we show the stimulation efficacy E in dependence of the applied power level P_{IN}. While there is no impact on cell growth at low power levels, the efficacy reaches its maximum $E = 1.13$ for $P_{IN} = 8$ mW, indicating a slightly but significantly increased cell migration rate. With increasing SAW intensity, however, the cell migration is impeded. At a high power level of $P_{IN} = 64$ mW, the rate is observed to decrease by as much as 20%.

Wave Mode. The results shown in Fig. 2*B* negatively answer the exciting question of whether also shear waves with particle displacement in the plane of the surface of the substrate only increase cell growth. In contrast to the successful stimulation with RWs at $P_{IN} = 4$ mW, there is only a slight and not significant increase of 8% for LW-mediated stimulation.

Pulsed Excitation. As under physiological conditions, pulsatile pressure fields can also appear, we exemplarily modulated the SAW intensity by the absolute values of the cardiac function $M(t)$ shown in Fig. 2*C*. The modulation frequency was set to $f = 1$ Hz, imitating the resting pulse ($\lambda_2 = 50$ µm). While the peak value is $P_{IN} = 16$ mW, the mean output is $\overline{P_{IN}} = 1$ mW. Using these settings, the power range between $0\ \text{mW} < P_{IN} < 16$ mW is covered, which leads to a positive effect for continuous SAW (CW) stimulation (Fig. 2*A*). However, as shown in Fig. 2*D*, only one out of five experiments resulted in a slightly positive effect, while on average, the cell growth is reduced as compared to the reference. Thus, in contrast to CW stimulation, an AM or pulsed SAW in the same power range has no or even a slightly negative impact on cell growth.

These data demonstrate that positive SAW-mediated cell stimulation strongly depends on the physical properties of the SAW. A wavelength of the order of the cell diameter and a vertical surface displacement component of the SAW for a gentle power level in the magnitude of $O(10^0$ mW) turned out to yield the strongest effects for SaOs-2 cells. The power dependency could be understood by the emerging negative effects accompanying SAW at high power levels: as shown earlier, there is a rise of substrate temperature of $\Delta T/\Delta P = 37$ K/W with increasing power (shown for $\lambda_1 = 25$ µm) (14). At a power level of

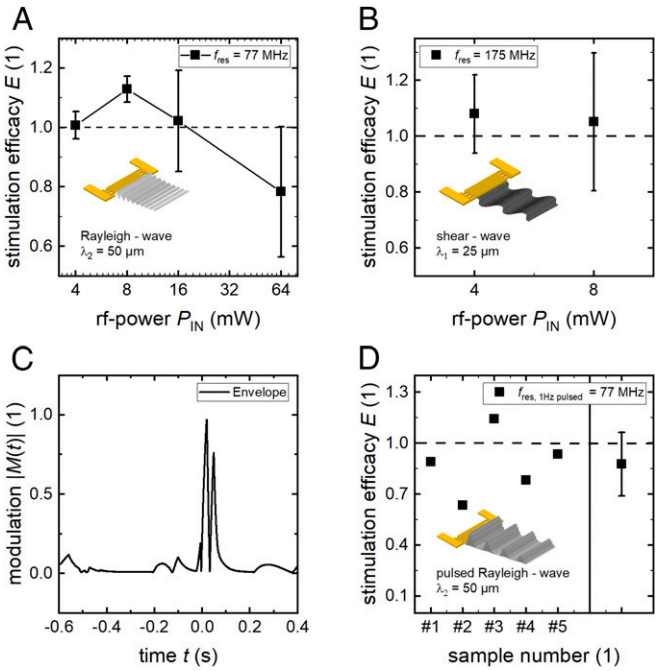

Fig. 2. SAW-stimulated cell growth at varying physical properties of the excited SAW. (*A*) Stimulation at different power levels at a wavelength of λ_2 = 50 µm (mean and SD of four independent measurements each). (*B*) Changing SAW mode to shear waves. (*C*) Amplitude-modulated signal for the pulsed modulation shown in *D*. The median time for surface coverage with SaOs-2 cells is about 60 h.

P_{IN} = 64 mW, a theoretical temperature rise of up to ΔT = 2.4 K is expected, where we assume an equal temperature rise for λ_1 and λ_2. However, this value exceeds the physiological temperature fluctuations and may harm the cells.

Conservation of SAW-Enhanced Cell Growth for Other Cell Lines and Collective Cell Migration. The experiments presented above used culture of SaOs-2 bone cancer cells. This mesodermal cell line has no polarity, a high motility, and gap junctions (28). Moreover, these cells, for their in vivo positions, do not necessarily require collective cell migration. In contrast, ectodermal cell lines have an apical and basal side forming a confluent cell layer with tight junctions. As one of their main purposes is to separate, to cover, and to protect the underlying tissue, the process of regeneration and wound-healing is essential. Therefore, a supported wound-healing not only for bone fractures but also for epithelial cells, as for example the dermis, would be highly interesting. To investigate the effect of SAW-mediated stimulation on ectodermal cells, in the following experiments, we used the model cell line MDCK-II.

Fig. 3*A* shows the invading cell front of MDCK-II cells 5 h after launching the SAWs and thus the stimulus. In contrast to the SaOs-2 cell species, MDCK-II cells migrate collectively, eventually establishing a clear and sharp edge of the cell layers. Moreover, this single snapshot already indicates a bulge in the vicinity of the aperture due to increased cell-migration velocity as a result of the SAW stimulation.

Between the electrodes of an IDT and within the traveling piezoactive SAW, large electrical fields up to O(1 kV/cm) are created. According to the model of Datta (29), the surface potential Φ is related to the acoustic power P_{SAW} described by the equation

$$P_{SAW} = \frac{1}{2}\frac{W}{\lambda_{SAW}} y_0 |\Phi|^2 \quad .$$

Here, W is the width of the aperture and y_0 the material-dependent characteristic admittance y_0 = 0.21 mS for $LiNbO_3$ and the cut used in our experiments. This results in a surface potential ranging from Φ = 0.3 V for P_{IN} = 1 mW up to Φ = 2.4 V for P_{IN} = 64 mW. Thus, the IDT can also be regarded as acting as a dipole transmitter. Therefore, cells in the vicinity of the electrode and along the SAW's sound path are stimulated by an electrical field. As reported earlier, electrical rf fields in the millihertz domain can actually act in an antiinflammatory manner and this way also promote the healing process (30). To separate the effect of electrical and mechanical stimulus, we performed reference measurements at a frequency f_{ref} = 100 MHz outside the bandwidth around the resonance frequency (f_{res} = 164 MHz). While the cells along the sound path at $f = f_{res}$ are stimulated mechanically and electrically in parallel (as illustrated in Fig. 3*B*), cells in the reference measurement at $f = f_{ref}$ only experience the electric fields of comparable frequency and intensity (as illustrated in Fig. 3*C*).

In Fig. 3*D*, the efficacy E at $f = f_{res}$ shows a pronounced increase in the power level range between P_{IN} ε [4 to 16 mW] with a maximum at P_{IN} = 8 mW. Cell growth in the SAW-stimulated area is up to 2.35 ± 0.73 times increased compared to the internal reference. The calculated P values in this interval are $P_{4\ mW}$ = 0.02, $P_{8\ mW}$ = 0.03, and $P_{16\ mW}$ = 0.03, concluding a significant increase at a 5% level of significance. Further increasing of the SAW-intensity I_{SAW} above 1 W/cm^2 results in a decrease of the efficacy E. This is in accordance with the observed decreased healing rate in US treatment mentioned above (12). However, no significant increase of the efficacy E can be determined for values $P_{IN} \geq 32$ mW. At power levels of P_{IN} = 128 mW and above, cells are either detached from the substrate surface or become necrotic within minutes to hours. Taken together, not in a single experiment was A_{mig} of the internal reference sections higher than A_{mig} in the sound path for values $P_{IN} \geq 2$ mW.

In contrast, there is no evidence for a positive stimulus at f_{ref} = 100 MHz, where no SAW is excited but a comparable electrical field is present. Here, the 5% level of significance is never reached for a single power level. For P_{IN} = 16 mW and higher, a slight effect in the reference measurements is observed. This could be understood by the generation of finite-amplitude SAWs even outside the bandwidth of the IDT for high power levels. In Fig. 4*A*, we depict the typical return loss S_{11} of an IDT as a function of frequency. While for this chip, the return loss at the resonance frequency is S_{11} = −18.59 dB, it is much weaker at the reference frequency with S_{11} = −0.93 dB. Thus, the intensity of the SAW for both frequencies f_{res} and f_{ref} differs by about 18 dB. Thus, at low power values, the SAW generation can safely be neglected at the reference frequency f_{ref}. However, increasing the applied power level eventually leads to an appreciable SAW generation but still much weaker as compared to the one at the resonance frequency f_{res} for the same applied power P_{IN}.

These findings are supported by the exemplarily shown superimposed images in Fig. 1 *D*, *d-1*–*d-3*. Here, the in vitro wound-healing process for a SAW-stimulated sample (Fig. 1 *D*, *d-1*), an electrical field-treated sample (Fig. 1 *D*, *d-2*), and an untreated sample (Fig. 1 *D*, *d-3*) is displayed. By comparing the three given images, the most pronounced cell migration is visible in the SAW-stimulated sample. Whereas the internal references exhibit reddish colors, the hues in front of the aperture appear to be violet and blue shaded. In contrast, in the next two images, only an electrical field was applied and an external reference with no stimulation indicates a uniform growth rate along the complete gap.

In analogy to previously published experiments (14), we applied RWs with a wavelength of 25 µm at power levels of P_{IN} = 2

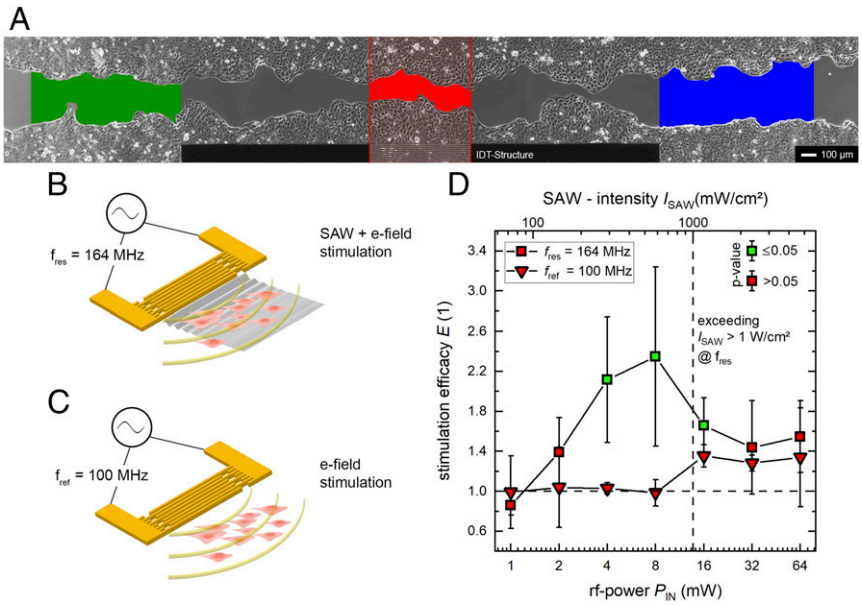

Fig. 3. SAW stimulation of the ectodermal cell line MDCK-II. (*A*) High-quality micrograph image of the progressive in vitro wound-healing in a confluent monolayer at $t = 5$ h. The colored regions indicate the SAW-stimulated cells (red) and the internal references (green and blue). (*B* and *C*) Representations of the different stimuli mechanism at different frequencies. While there is a simultaneous mechanical and electrical stimulation at the SAW resonance frequency, we depict in *B* the result of an electrical stimulus only. This is achieved by detuning the IDT frequency to a somewhat lower value outside its bandwidth, where no SAW is excited (*C*). (*D*) Power dependency on SAW stimulation at different frequencies. There is significant improvement of cell growth and migration rate up to 135 ± 85% for SAW-supported cell growth at $P_{IN} = 4$ and 8 mW. Exceeding $I_{SAW} > 1$ W/cm^2 leads to a decrease of stimulation efficacy *E*. A significant increase of the efficacy ($P < 0.05$) compared to an external low control is indicated by the color of the symbols' inner area. The median time for surface coverage with MDCK-II cells is about 31 h.

and 4 mW to SaOs-2 cells. However, we additionally added a 10-nm-thick conductive titanium layer on top of the sound path, as indicated in *SI Appendix*, Fig. S3. Compared to the same experiments but without a shielding layer, no significant difference in increase of cell growth was found (15 ± 2 vs. 12 ± 5%). In these experiments the mechanical stimulation nearly remains unchanged, but lateral electrical fields are shortened completely and vertical electrical fields are shielded to some extent. These data further support our conclusions excluding electrical fields as a major contribution to the observed effect.

Further indications that the electrical fields are no major contributor to the effect are the results shown in Fig. 2*B*. Shear waves are accompanied by electrical fields of the same order of magnitude but do not lead to significantly increased in vitro wound-healing.

Moreover, we performed additional reference measurements regarding the agitation of medium. Here, the IDT (λ_{SAW} = 25 µm) is placed alongside the gap, inducing streaming by leaky SAWs at a power level of $P_{IN} = 4$ mW. Therefore, the cell culture is only affected by the streaming. A comparison to external references without SAW application running in parallel demonstrates no significant impact on the cell growth ($E = 0.97 \pm 0.33$). For further details, see *SI Appendix*.

However, to allow for quantitatively comparing the SAW-induced streaming with the literature and to understand the cell-stimulating mechanical forces, the well-known acoustic streaming effect (31) that is proportional to the SAW intensity is measured quantitatively. Fig. 4*B* shows the flow profile evaluated at a height $h = +25$ µm above the substrate measured by sPIV. The liquid is drawn toward the IDT and then streams upward under the Rayleigh angle. Mean velocities are measured for both the SAW-illuminated region and the internal reference. Both regions are compared in Fig. 4*C*, while the mean flow speed near the center of the artificial wound in front of the aperture is labeled with * and parallel in the internal reference with **. As expected for $f = f_{res}$, the velocity increases linearly with the applied power level until it reaches its measured maximum of v_{as} = 1.2 mm/s at $P_{IN} = 128$ mW. For $f = f_{ref}$, only slight streaming appears for $P_{IN} \geq 32$ mW. For $P_{IN} = 128$ mW, the acoustic streaming velocity (v_{as}) is comparable to the one at f_{res} at $P_{IN} = 1$ mW at the magnitude of O(10^{-2} mm/s).

The maximum velocity of $v_{as} = 1.2$ mm/s results in a dynamic pressure q:

$$q = \frac{\rho}{2} v^2 = 6.05 \cdot 10^{-4} \text{Pa},$$

and a shear stress τ:

$$\tau = \eta \frac{\Delta v_{as}}{\Delta z} = 0.47 \quad \frac{\text{Ç}}{\text{dyn/cm}}.$$

Here, ρ reflects the density of water and $\eta = 0.97$ cP the viscosity of medium with 10% fetal bovine serum at $T = 37$ °C (32). If the observed effect was only a simple result due to streaming, the flow field generated here would result in an asymmetric artifact in the observed cell migration: cells on the IDT side, denoted as the "downstream" side, have to migrate against the direction of flow, while the opposing cells migrate along the flow, denoted as "upstream." This would result in a nonuniform, even asymmetric wound closure. To identify such possible differences in the migration speed, as illustrated in Fig. 4*E*, the velocities of both opposing cell fronts (luv and lee) are shown in Fig. 4*D*. All data points scatter around the bisector with a very slight tendency to the upper side.

The ratio $v_{IDT\text{-}side}/v_{IDT\text{-}opp}$ is smaller than 1 for 65% of the data points for f_{res} and 59% for f_{ref}, respectively. The average values are $v_{IDT\text{-}side}/v_{IDT\text{-}opp} = 1.08 \pm 0.67$ and $v_{IDT\text{-}side}/v_{IDT\text{-}opp} = 0.95 \pm 0.61$ for SAW and electrical-field stimulation, respectively. This indicates that the streaming effect on cell migration is

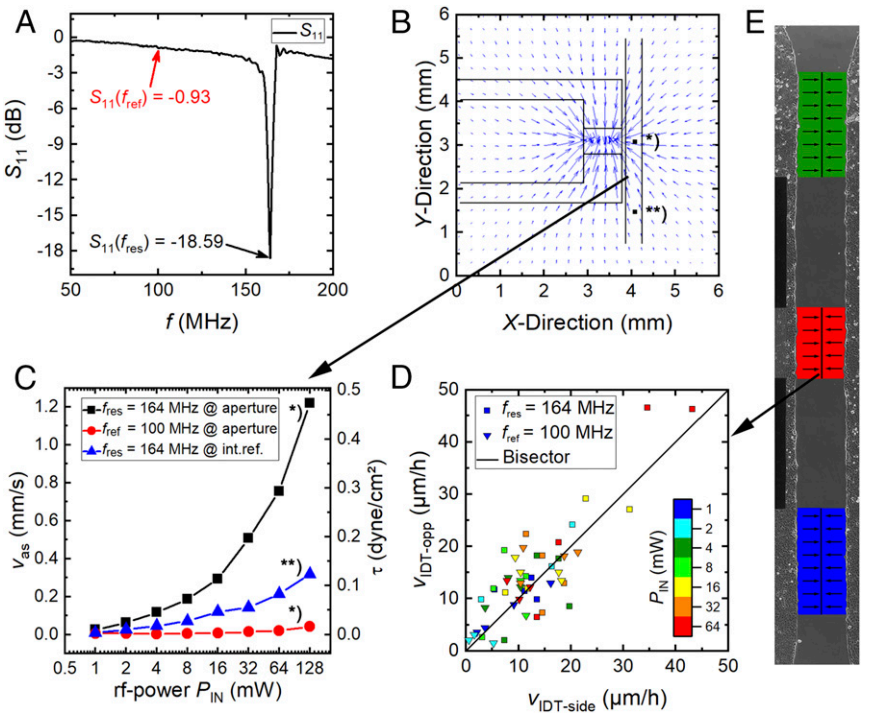

Fig. 4. Physical properties of the experimental setup and the cellular response. (*A*) The return loss S_{11} is strongly frequency-dependent. While for $f = f_{res}$, a SAW is resonantly excited, at $f = f_{ref}$, only the electric field stimulates the cells. (*B*) To estimate the SAW-intensity at different power levels P_{IN} and to characterize the flow profile, an sPIV measurement was performed at a height h = +25 µm above the substrate. The liquid is streaming toward the aperture. The streaming velocity (v_{as}) was determined at the aperture * and the internal reference **. (*C*) Power- and location-dependent streaming velocity $v = v_{as}$. (*D*) The small asymmetry of the flow profile has no significant impact on the migration velocities of the opposing cell fronts in *E*.

indeed weak and thus can be neglected in our data analysis. If the cells migrate faster, this holds for both sides of the gap.

These data demonstrate the positive effect of SAW stimulation on cell growth. In a narrow SAW power interval, a significant increase of the surface-coverage rate can be observed, where lower intensities have no significant impact and very high intensities are observed to impede the cell growth. Furthermore, the comparison between the SAW-stimulated area and the internal reference strongly support the assumption that only the mechanical component of the piezoactive SAW is the main reason for the effect and is not outweighed by spurious, accompanying side effects like temperature, fluid flow, or electrical fields.

Possible reasons for our findings could be an enhanced proliferation or an increased cell activity as well as an increased cell migration for cells residing in the sound path. To narrow down the underlying mechanisms and to characterize potentially negative impacts of the SAW stimulation on cells at very high SAW intensities, the proliferation of cells and the production of intracellular ROS was analyzed.

The Influence of SAW Stimulation on Intracellular Mechanisms. In order to understand the significant increase of the stimulation efficiency for MDCK-II cells at P_{IN} = 4 to 8 mW, cellular parameters, like cellular stress and proliferation, are measured by fluorescence imaging. ROS are indicators of cellular stress and play a significant role in programmed cell death or necrosis by activating signal cascades and inducing or suppressing gene expression (33). Therefore, they are a valuable indicator to determine negative side effects of SAW stimulation. In contrast, proliferation in healthy cells is an actively controlled mechanism and is regulated by multiple signals, ranging from growth factor signaling to DNA damage, developmental cues (34), mechanical manipulation (35), and spatial restrictions (36, 37). In these experiments, we extended the power range and also included a very high power level of P_{IN} = 128 mW to explore the limits of SAW stimulation.

Stress Level: ROS. In our experimental setup, both mechanical forces and possible thermal effects induced by the high SAW intensities act on the whole cell culture. To qualify any potential negative effects, the concentration of ROS in the cells residing within the SAW-inflicted area is compared to the internal reference as well as an external "low" and "high" control. In *SI Appendix*, a typical image of the intracellular stress of SAW-stimulated cells at a power level of P_{IN} = 64 mW is shown. The quality of the cell layer and possible morphological changes are verified for each sample using phase-contrast imaging. No morphological changes were identified for values $P_{IN} \leq 64$ mW. The position information of the nuclei in selected regions is used to determine the cellular stress level as a function of the applied power level P_{IN}, as displayed in *SI Appendix*, Fig. S5. For the complete power range tested, the experimental conditions of the cells close to the aperture remain the same as for the internal reference or low control. Therefore, there is no significant increase of ROS due to SAW stimulation for the tested power range between P_{IN} = 8 mW and P_{IN} = 64 mW. At very high SAW powers (P_{IN} = 128 mW), some cells start to become ripped off of the substrate inter alia caused by the high shear stress induced by the acoustic streaming. Furthermore, the cell-coverage rate is significantly decreased for the complete culture, as can be seen from the gap still being present after 24 h. At high intensities, the temperature in the culture media increase due to a SAW-related substrate heating. At a power level of P_{IN} = 128 mW, the abovementioned substrate heating, for example, results in an increase of the bulk media temperature from about $T_{P=0\ mW}$ = 36.6 °C to $T_{P=128\ mW}$ = 39.1 °C, thus exceeding the ideal culture

conditions. Therefore, the data points for P_{IN} = 128 mW are poorly suited for this measurement, and this power value marks a threshold: for higher intensities, like, e.g., P_{IN} = 256 mW, cells become necrotic and are removed from the substrate in the area around the aperture.

This concludes that there is no SAW-induced increase of intracellular ROS for a reasonable range of power levels ($P_{IN} \leq 64$ mW). The cellular stress level remains in the normal range, as proven by the identical condition of treated and untreated cells for ideal SAW parameters, as shown before in *Conservation of SAW-Enhanced Cell Growth for Other Cell Lines and Collective Cell Migration*.

Proliferation. The proliferation of cells is regulated and stimulated by mechanical forces, electrical stimulation, spatial restrictions, and others mechanisms (35, 37, 38). We demonstrate a positive impact of SAW on the proliferation rate in the SAW-irradiated samples. Since not only cells in the sound path but also in the internal reference are stimulated, enhanced proliferation can be excluded as the main reason for the increased efficacy *E* shown above in *Conservation of SAW-Enhanced Cell Growth for Other Cell Lines and Collective Cell Migration*.

For a conclusive evaluation, the proliferation rate was determined along the SAW sound path at the artificial wound and inside the confluent cell layer and compared to the corresponding internal and external reference. In Fig. 5*A*, proliferated cells of a large area around the IDT structure are displayed. In the upper section of Fig. 5*A*, the tapering of the cell layer marks the section of the former gap, while the lower section shows the domain of the initial cell layer. Selected regions indicated by the colored rectangles (Δx = 300 μm; Δy = 650 μm) are evaluated in accordance with the ROS measurements. Red marks the "front aperture" area and blue the "rear" of the aperture. Yellow and green, respectively, indicate the corresponding "internal references." Fig. 5 *B–D* displays a section of the cell layer in front of the aperture. The phase-contrast image in Fig. 5*B* is used to verify the cell layer's quality, while Fig. 5*C* shows the nuclei of all cells and Fig. 5*D* only the cellular nuclei with freshly synthesized DNA. The labeled areas are evaluated statistically, as described previously in *Stress Level: ROS*. Each measurable is depicted as a

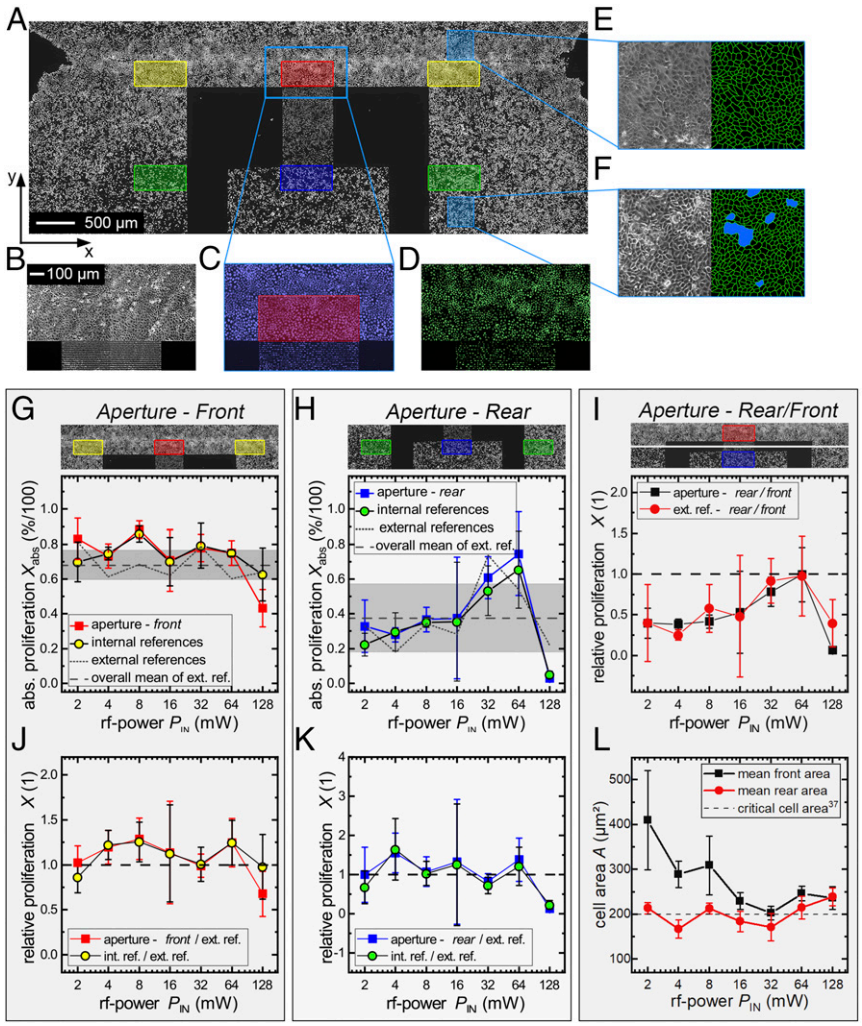

Fig. 5. Determination of the SAW-induced influence on cell proliferation. (*A*) Fluorescence image of nuclei with newly synthesized DNA with evaluated regions marked in different colors (red: front aperture; yellow: internal reference front; blue: rear aperture; green: internal reference back). (*B–D*) Images of the artificial wound in phase contrast (*B*), all cellular nuclei (*C*), and newly synthesized (*D*). (*E* and *F*) Phase-contrast images and cell border of the cell layer. (*E*) MDCK-II at low density (wound). (*F*) MDCK-II at high density with emerging cell domes (blue spots). (*G* and *H*) Absolute proliferation $X_{abs}(P_{IN})$ of the front and rear area. (*I*) Relative proliferation inside the cell layer and at the edge. (*J* and *K*) SAW-stimulated samples compared to external references. (*L*) Average area per cell in the corresponding external reference in the front and rear section of the aperture. Cultivation time for measurement point at P_{IN} = 16 mW is t = 22 h; otherwise, t = 27 h.

small inset above the corresponding graphs. All data points for one power level represent samples from the same cell passage prepared on the same day. In the external references, no SAW was employed at all, although the rest of the setup was prepared analogously to the other samples. Fig. 5 *G* and *H* shows the absolute proliferation rate depending on the applied power level P_{IN} in the front and rear of the aperture. The gray shaded areas correspond to the SD of all external references. Fig. 5*I* shows the relations between the front and rear region of the IDT in the sample and in the external reference. Fig. 5 *J* and *K* displays a comparison on the relative proliferation rate $X(P_{IN})$ between the samples and the external references. For the consideration of the actual cell density, Fig. 5*L* characterizes the postmitotic mean area per cell A in the external references independent from eventual SAW-induced stimulation effects.

In Fig. 5 *G* and *H*, the course of the absolute proliferation X_{abs} in the stimulated area in the sound path is nearly identical to the internal reference for a wide range of the applied power levels P_{IN} for both the front and the rear side of the IDT. In Fig. 5*G*, distinct maxima for $X_{abs\text{-}aperture}(8\ mW) = 0.88 \pm 0.05$ and $X_{int.\ ref.}(8\ mW) = 0.86 \pm 0.05$, respectively, are observed as compared to the external reference $X_{ext.\ ref.}(8\ mW) = 0.68 \pm 0.12$. Furthermore, at a very high power level $P_{IN} = 128$ mW, a significant decrease in the front aperture becomes visible $X_{abs\text{-}aperture}(128\ mW) = 0.43 \pm 0.11$.

Thus, we state that there is no significant difference in the proliferation rate of cells in the sound path to cells in the internal reference. However, an increase of $X(P_{IN})$ is ascertainable when considering the proliferation of the treated samples relative to the external reference. $X(P_{IN})$ is increased for a wide range between $P_{IN} = 4$ mW and $P_{IN} = 64$ mW, as shown in Fig. 5*J*. The maximum values are reached at $P_{IN} = 4$ and 8 mW, with P values of $P_{4\ mW} = 0.058$ and $P_{8\ mW} = 0.049$, which correspond to the maximum for the surface-coverage rate of Fig. 3*D*. At $P_{IN} = 128$ mW, the relative proliferation rate decreases only at the aperture to $X(128\ mW)_{rel\text{-}SAW} = 0.68$ ($P_{128\ mW} = 0.033$) in contrast to the internal reference $X(128\ mW)_{rel\text{-}int.\ ref.} = 0.98$. For cells inside the layer (Fig. 5*K*), this effect is not very pronounced, but still a significant increase of X_{rel} is measurable for $P_{IN} = 4$ mW with $X_{rel\text{-}SAW}(4\ mW) = 1.55 \pm 0.51$ ($P_{4\ mW} = 0.027$) and a decrease for $P_{IN} = 128$ mW with $X_{rel\text{-}SAW}(128\ mW) = 0.053 \pm 0.226$ ($P_{4\ mW} = 0.034$).

The comparison of the absolute values in the sound path at the front with the proliferation rate inside the layer obviously exhibits fluctuations (Fig. 5*H*). Cells in the front always proliferate more than in the back. Here, SAW-dependent effects can be excluded as the external reference shows the same course (Fig. 5*I*). This might be a consequence of the actual state and density of the cell culture for the day of the experiment. Cells at the edges, moreover, can cover a larger surface than cells inside the layer (Fig. 5*L*).

If we compare the mitosis of the cells at the edges of the layer having a low areal density to those cells being tightly packed in the layer, we observe a continuously higher proliferation rate (Fig. 5*I*) for the first. This matches the fact that the division rate is known to slow down with decreasing cell-free space. Puliafito et al. (37) reported on a critical cell area of about $A_{crit} = 200\ \mu m^2$, below which the cell division rate dramatically decreases. They argue that this decrease is due to cell-contact inhibition. As cells at the edges of the cell layer can acquire more space, they proliferate more than cells inside of the layer. As shown exemplarily in Fig. 5 *E* and *F*, the available space per cell in the gap area after 27 h with a median of $A = 193\ \mu m^2$ is still larger than the one in the interior of the layer with $A = 170\ \mu m^2$. In Fig. 5*F*, we depict the appearance of cell domes (marked in blue) because of the high cell density. The phenomenon of contact inhibition (37) can also explain the distinctive drop in the relative proliferation rate at $P_{IN} = 16$ and 32 mW in Fig. 5*J*. In these distinct experiments, a spatially confined impairment of the cell proliferation occurred due to a cell density that was accidentally too high in the critical cell area range. Note that the proliferation rate in the rear section of the sound path is significantly increased to $X(4\ mW) = 1.55 \pm 0.51$ ($P_{4\ mW} = 0.027$) even though the cell density fluctuates around A_{crit} in the sample as well as in the internal reference.

Our data are clearly consistent with a significant effect of SAW stimulation on the proliferation of cells. Cells being actively irradiated by SAW proliferate up to $29 \pm 23\%$ more than in the external reference. The fact that cells in the internal reference proliferate similarly to the ones in the sound path is attributed to streaming effects. As there is a measurable flow in the whole culture, as shown in Fig. 4*C*, the cell medium is actively stirred (23), reducing the local metabolite concentration and increasing the gas exchange as compared to a diffusion-limited static culture (39). The obvious decrease for high power levels at $P_{IN} = 128$ mW may result from high shear forces simply detaching the cells from the substrate. While cells in the interphase are firmly attached to the culture surface, cells round up in the mitotic phase and are therefore much more loosely attached to the surface (40). The acting shear stress of about $t \sim 0.47$ dyn/cm^2 for the measured streaming velocity of $v = 1.2$ mm/s at $P_{IN} = 128$ mW is apparently high enough to remove mitotic cells in the vicinity of the aperture. This subsequently results in a decreased proliferation rate. Furthermore, as explained in the ROS measurements, any SAW-induced temperature increase of the media could harm the cells.

Greco et al. (20) recently demonstrated positive and negative effects on cell proliferation upon SAW stimulation, also depending on two distinct applied power levels. Our data, however, presume a two-stage threshold effect for a wide power range. Remaining largely unmodified for low SAW intensities, the proliferation rate $X(P_{IN})$ increases if the SAW-induced media stirring is strong enough. The rate is independent from the actual streaming velocity and SAW power level P_{IN}, as long as the diffusion limitation for media supply is overcome. After reaching a second threshold, the effect reverses and the proliferation is decreased.

The fact that the proliferation in the whole culture is positively affected by the SAW treatment suggests that proliferation alone cannot be the cause for the increased surface coverage of cells in the sound path compared to the internal reference.

Discussion

The results of this study clearly indicate the high impact of SAW-mediated cell stimulation on the closure of an artificial wound in a cell monolayer in a distinct power range. The surface-coverage rate in the sound path is increased up to 135%, compared to an internal reference and depending on the experimental conditions. For the increased surface-coverage rate, a variety of different mechanisms like increased proliferation, cell activation, or enhanced cell spreading and migration may be considered. In earlier wound-closure studies (41, 42), cell spreading and migration rather than enhanced proliferation had already been assigned to be the major mechanisms for in vitro wound closure.

In the following, we exclude enhanced proliferation or acting shear forces as the main reasons at low power levels for the increase in stimulation efficacy. Then, we narrow down the remaining cause of the observed effect to increased cell migration evoked by the mechanical, not electrical, component of the SAW. Moreover, we discuss that this mechanical stimulation can influence the intracellular calcium concentration and therefore the migration rate. Finally, we argue that a mechanic stimulation also can explain negative effects for a pulse modulation.

As we find an increased cell proliferation on the whole chip rather than only in the sound path, a higher mitotic rate can be ruled out for our findings of increased wound-healing in the

sound path. Therefore, only cell migration and spreading may be the reason for increased surface coverage. Reasons for an enhanced migration vary widely and can be influenced by signaling molecules, cell activation state, or external forces. For instance, it has been suggested that wounding, as given in our case, causes the release of signaling molecules or growth factors to promote cell motility (43). Laminar flow toward the IDT should promote the convective transport of chemokines to cells on the IDT side to enhance the migration. Since both sides migrate in the same manner, it is unlikely that enhanced cell migration was due to an enhanced transport of signaling molecules.

Another point to consider is cell stimulation evoked by shear flow. As shear forces are important modulators of endothelial cells, they influence important functions like cell elongation, formation of stress fibers, increased permeability, secreting chemoattractants, activation of G proteins, and so forth (44, 45). However, the cellular alteration depends on the shear magnitudes: distinct changes in cell morphology and orientation (>8 dyn/cm^2) (46, 47), chemoattractant secretion (>9.8 dyn/cm^2) (48), influenced migration direction (>3 dyn/cm^2) (49), activation of protein kinases (>0.5 dyn/cm^2) (50), or inhibition of apoptosis (>15 dyn/cm^2) (51). Furthermore, it has been shown that low shear rates (<4 dyn/cm^2) can enhance proliferation and differentiation for osteoblasts and fibroblasts (52–54). Concerning the cell migration, Hsu et al. (55) demonstrated, for high shear stresses (17 dyn/cm^2), an increased migration rate at wound edges for laminar and disturbed flow conditions compared to static cultures. Especially laminar flow facilitates cell migration by promoting of cell–cell junction disruption and focal-adhesion dynamics or mechanical-pushing effects. Furthermore, intracellular signaling pathways like small GTPase Rho and tyrosine kinases are stimulated under high shear conditions, promoting cell motility (55).

In the power range of P_{IN} = 4 to 8 mW, the maximal shear stress is 0.07 dyn/cm^2 and consequently, based on literature cited previously (44–55), too small to remarkably stimulate cells. If the effect was simply a consequence of shear stress, the absolute values of the surface-coverage rate for the internal references would have to increase with increasing power. This is not the case. Induced activation through shear forces are therefore also out of the question.

However, for higher values above $P_{IN} \geq 32$ mW, the effective shear force exceeding 0.2 dyn/cm^2 might no longer be negligible. Cells may be stimulated, inducing, e.g., the activation of protein kinases. However, at the same time, negative effects due to a temperature increase might appear.

A local-substrate heating results in a linear increase of the substrate temperature $\Delta T_s = 37 \frac{\text{mK}}{\text{mW}} P_{IN}$ for power levels below 100 mW. Therefore, at values $P_{IN} \geq 32$ mW, the temperature increase can exceed the physiological fluctuations of ~±1 K what might harm the cell.

Thus, at high power values, cells in the sound path are simultaneously affected by positive and negative influences ($I_{SAW} > 1$ W/cm^2; $T_s > 38$ °C). The cells in the internal reference may also be positively affected by the increased shear force ($\tau >$ 0.1 dyn/cm^2 for P_{IN} = 128 mW). This might result in an overall decreased relative efficacy E for high power values.

Consequently, we exclude enhanced proliferation or acting shear forces as the main reasons at low power levels for the increase in stimulation efficacy. Up to this point, increased cell migration evoked by mechanical or electrical stimulation remains as the only possible and plausible cause. As there is no evidence for cell stimulation at f_{ref} (Fig. 3*D*), the electric component of the SAW can also be excluded.

This leads to the question of how cells could react on such a mechanical stimulation. Through the mechanical component of a SAW, cells along the sound path undergo mechanical vibration, pressure, and deformation forces. By the fact that most cells are mechanosensitive (56, 57), a cellular response on these acting forces can be expected. A possible response would be a change in the intracellular calcium concentration $[Ca^{2+}]_i$. In previous studies, it has been demonstrated that $[Ca^{2+}]_i$ can be increased by mechanically stimulating the cell membrane with a microprobe by discrete membrane deformation or stretching of the cell membrane (58–60). If cells grow in a confluent monolayer, adjacent nonstimulated cells also show an increase of $[Ca^{2+}]_i$ up to a radius of four to six cells or a distance of up to 100 μm (58). As calcium $[Ca^{2+}]_i$ is well known to play a crucial role in regulating cell migration (studies: refs. 61 and 62; reviews: refs. 63–65), the mechanically induced calcium release could be a possible reason for the enhanced cell motility. The transmission of the Ca^{2+} response across a confluent monolayer may explain the increased motility of nonstimulated cells in the vicinity of the sound path. In contrast, cells at the internal reference are too far apart to become influenced by SAWs. The ineffectiveness of LWs can be traced back to the missing z-deflection of the substrate as LWs are polarized horizontally and therefore missing substrate vibration. Summing up, a change of the intracellular calcium concentration can explain our observation.

Last but not least, a mechanical stimulation mechanism can help to understand the observed decreased efficacy for pulsed stimulation. Cells can adapt to mechanical stress by reorganizing the cytoskeletal structure or cell shape (66). Among other things, the cytoskeletal stiffness is increased in direct proportion to the applied stress (67). Dependent on the applied force shape and thus time constant, the cellular adaptation ranges from an immediate viscoelastic response, adaptive behavior with oscillatory forces, and adaptive cell stiffening of adhesion structures with sustained static stress (>15 s) to large-scale repositioning response with prolonged (>1 min) stress (68). This may explain the adverse effect of pulsed SAW on cell growth. Applying a constant force results in improved cellular adaptation compared to short 1-Hz pulses.

For future studies answering the remaining open questions, from a biochemical point of view, it is crucial to find a human cell line with a high transfection efficiency. We thus treated T-REx-293 in identical experiments as described above (P_{IN} = 8 mW; λ_{SAW} = 25 μm). Here, we obtained a stimulation efficiency of $E = 1.24 \pm 0.08$ (n = 4; P = 0.0003). This further supports the claim that the observed effect is not limited to one or two single cell lines and opens up a whole range of possibilities to modify the studied cell line, to further narrow down the stimulation mechanism.

In total, the stimulation mechanism is a combination of substrate movement and shear stress. Depending on the applied power level P_{IN}, the respective contribution on cell stimulation may differ. While at low power levels, cells are positively affected only by mechanical vibration, the contribution of shear forces and temperature can no longer be neglected for higher values and the positive effect turns around if the applied power level is too high. How the mechanotransduction of this stimulation in the megahertz regime actually takes place in detail has to be further illuminated. It might contain even a "rectifying" direct-current (DC) effect (cf. acoustic streaming), acting via the pressure dependent density on the cell membrane and thus also the interior of the cell. Such a potential DC effect indeed would be consistent with the ineffectiveness of LWs, as they do not excite waves into the medium. As we are still unable to really prove such hypotheses, we do not claim a specific mechanism here.

Conclusion and Outlook

We here presented an in-depth study of SAW-mediated cell growth for tissue stimulation and wound closure. We employed SAW with different parameters on different cell lines and successfully identified their relevance in terms of enhanced cell growth. As addressed in *Identifying the Most Relevant SAW*

Parameters for Cell Stimulation, there exist manifold possibilities to vary the SAW parameters, and due to their interdependence, several tests do not depend on a single parameter. Within the covered range of parameters, RWs with a wavelength of the order of the size of the adherent cells are found to be most efficient in their influence on the cell growth. While employing a wide power range of the SAW, we identify a global maximum of the stimulation efficacy. For SaOs-2 cells, for example, this maximum turns out to be $E = 1.18$ for $P_{IN} = 8$ mW. For MDCK-II cells, for comparison, we find an even larger increase of up to 135% (compared to the internal reference) in the power interval of $P_{IN}\ \varepsilon$ [4 to 16 mW].

As SAWs on a piezoelectric substrate contain both the mechanical as well as electrical components, we measure the surface-coverage rate at the SAW resonance frequency and a slightly different excitation frequency, where no SAW is generated but the electric fields around the transducer are basically the same. The fact that SAW-treated cells in the sound path at f_{res} migrate faster as compared to the "no-SAW" frequency f_{ref} confirms our hypothesis that the mechanical component is decisive for an enhanced surface coverage.

Besides the main effect shown here, this technology also enables additional studies focusing on the extremely low shear-force regime within one cell ensemble. A correlation of flow field and various cell responses could be performed in a similar manner, as presented earlier, for example, with cell adhesion (69).

To understand the intracellular mechanisms, which leads to an increased migration rate, the concentration of ROS and the proliferation of cells were measured. While the cellular stress remains equal to the low controls for the measured power spectra, a significant change in the proliferation for the whole stimulated sample was noticed. We demonstrated a two-step threshold for the proliferation. Remaining unmodified for low SAW intensities, the proliferation increases for values above $P_{IN} \geq 4$ mW up to $29 \pm 23\%$ compared to the external reference. Reaching a second point, $P_{IN} \geq 128$ mW, excessive SAW intensities subsequently led to a decrease in the measured proliferation. The reasons for the increased in vitro wound-healing are therefore not an increased proliferation rate of cells in the sound path, as all cells on the chip proliferate faster.

The exclusion of proliferation, ROS, temperature, shear force, and electrical fields identifies the mechanical stimulation by vibration as the main cause for our observed phenomena of further enhanced in vitro wound-healing, in addition to overall increased proliferation.

Since cells can adapt to mechanical stress by reorganizing the cytoskeletal structure or cell shape (66), further studies should investigate the impact of known factors that regulate cytoskeletal structure or cell shape. Recently, for instance, an intramembrane protease was implicated in the regulation of protein glycosylation (70, 71), which strongly impacts the composition of the extracellular matrix and, thus, cytoskeletal structure and cell shape. Furthermore, it would be highly interesting to determine the calcium response, cell activation, or biomarker expressions. As cells, especially stem cells, are influenced by the stiffness of the substrate (72), an application of SAW stimulation to influence differentiation would be very illuminating.

Transferring this fundamental result to a medical application, of course, is a completely new and additional task. Rough ideas of how this could be managed are arrays of transducers on flexible disposable substrates (73) that are inductively power supplied (74). Going even one step further could be transducers on implants that are supplied in the same way.

Data Availability. All study data are included in the article, *SI Appendix*, and Movies S1–S3.

ACKNOWLEDGMENTS. We thank the Cluster of Excellence "Nanosystems Initiative Munich" and the Augsburg Centre for Innovative Technologies for funding. This work was funded by the German Research Foundation (DFG, Deutsche Forschungsgemeinschaft) – 263531414/FOR 2290 and 254872893/FL 635/2-2. We also thank Sidonie Lieber, Alexander Hupfer, and Andreas Hörner for technical assistance and Emeline Nysten for scanning electron microscopy of SAWs. M.S.B. thanks the "Stiftung der deutschen Wirtschaft" for personal funding.

1. S. Buchegger *et al.*, Antibacterial metal ion release from diamond-like carbon modified surfaces for novel multifunctional implant materials. *J. Mater. Res.* **31**, 2571–2577 (2016).
2. A. Stejskalová, N. Oliva, F. J. England, B. D. Almquist, Biologically inspired, cell-selective release of aptamer-trapped growth factors by traction forces. *Adv. Mater.* **31**, e1806380 (2019).
3. H. G. Knoch, Beitrag zur Wirkungsweise der Ultraschallenergie. *Schriften der Med. Akad. Dresden* **6**, 81–87 (1967).
4. W. Klug, W.-G. Franke, H.-G. Knoch, Scintigraphic control of bone-fracture healing under ultrasonic stimulation: An animal experimental study. *Eur. J. Nucl. Med.* **11**, 494–497 (1986).
5. T. K. Kristiansen, J. P. Ryaby, J. McCabe, J. J. Frey, L. R. Roe, Accelerated healing of distal radial fractures with the use of specific, low-intensity ultrasound. A multicenter, prospective, randomized, double-blind, placebo-controlled study. *J. Bone Joint Surg. Am.* **79**, 961–973 (1997).
6. A. Binder, G. Hodge, A. M. Greenwood, B. L. Hazleman, D. P. Page Thomas, Is therapeutic ultrasound effective in treating soft tissue lesions? *Br. Med. J. (Clin. Res. Ed.)* **290**, 512–514 (1985).
7. J. D. Heckman, J. P. Ryaby, J. McCabe, J. J. Frey, R. F. Kilcoyne, Acceleration of tibial fracture-healing by non-invasive, low-intensity pulsed ultrasound. *J. Bone Joint Surg. Am.* **76**, 26–34 (1994).
8. A. A. Pilla *et al.*, Non-invasive low-intensity pulsed ultrasound accelerates bone healing in the rabbit. *J. Orthop. Trauma* **4**, 246–253 (1990).
9. M. Dyson, M. Brookes, Stimulation of bone repair by ultrasound. *Ultrasound Med. Biol.* **2** (suppl. 2), 61–66 (1983).
10. D. P. Zachs *et al.*, Noninvasive ultrasound stimulation of the spleen to treat inflammatory arthritis. *Nat. Commun.* **10**, 951 (2019).
11. C. L. Tsai, W. H. Chang, T. K. Liu, Preliminary studies of duration and intensity of ultrasonic treatments on fracture repair. *Chin. J. Physiol.* **35**, 21–26 (1992).
12. R. Williams, Production and transmission of ultrasound. *Physiotherapy* **73**, 113–116 (1987).
13. D. L. Miller *et al.*; Bioeffects Committee of the American Institute of Ultrasound in Medicine, Overview of therapeutic ultrasound applications and safety considerations. *J. Ultrasound Med.* **31**, 623–634 (2012).
14. M. E. Stamp, M. S. Brugger, A. Wixforth, C. Westerhausen, Acoustotaxis - In vitro stimulation in a wound healing assay employing surface acoustic waves. *Biomater. Sci.* **4**, 1092–1099 (2016).
15. A. Rathgeber, C. Strobl, H.-J. Kutschera, A. Wixforth, Planar microfluidics–Liquid handling without walls. *J. Colloid Interface Sci.* **357**, 534–540 (2001).
16. X. Ding *et al.*, On-chip manipulation of single microparticles, cells, and organisms using surface acoustic waves. *Proc. Natl. Acad. Sci. U.S.A.* **109**, 11105–11109 (2012).
17. A. Hartmann *et al.*, A novel tool for dynamic cell adhesion studies - The De-Adhesion Number Investigator DANI. *Lab Chip* **14**, 542–546 (2014).
18. D. J. Collins *et al.*, Two-dimensional single-cell patterning with one cell per well driven by surface acoustic waves. *Nat. Commun.* **6**, 8686 (2015).
19. M. S. Brugger *et al.*, Orchestrating cells on a chip: Employing surface acoustic waves towards the formation of neural networks. *Phys. Rev. E* **98**, 012411 (2018).
20. G. Greco *et al.*, Surface-acoustic-wave (SAW)-driven device for dynamic cell cultures. *Anal. Chem.* **90**, 7450–7457 (2018).
21. R. M. White, F. W. Voltmer, Direct piezoelectric coupling to surface elastic waves. *Appl. Phys. Lett.* **7**, 314–316 (1965).
22. D. Morgan, *Surface Acoustic Wave Filters* (Elsevier, 2007).
23. K. Sritharan, C. J. Strobl, M. F. Schneider, A. Wixforth, Z. Guttenberg, Acoustic mixing at low Reynold's numbers. *Appl. Phys. Lett.* **88**, 1–3 (2006).
24. K. Dransfeld, E. Salzman, Excitation, detection, and attenuation of high-frequency elastic surface waves. *Phys. Acoust. Princ. Methods* **7**, 219–272 (1970).
25. F. G. Strobl *et al.*, A surface acoustic wave-driven micropump for particle uptake investigation under physiological flow conditions in very small volumes. *Beilstein J. Nanotechnol.* **6**, 414–419 (2015).
26. R. W. Rambach, V. Skowronek, T. Franke, Localization and shaping of surface acoustic waves using PDMS posts: Application for particle filtering and washing. *RSC Advances* **4**, 60534–60542 (2014).
27. P. K. Maini, D. L. S. McElwain, D. I. Leavesley, Traveling wave model to interpret a wound-healing cell migration assay for human peritoneal mesothelial cells. *Tissue Eng.* **10**, 475–482 (2004).
28. S. B. Doty, Morphological evidence of gap junctions between bone cells. *Calcif. Tissue Int.* **33**, 509–512 (1981).
29. S. Datta, *Surface Acoustic Wave Devices* (Prentice-Hall, 1986).
30. D. Foley-Nolan *et al.*, Low energy high frequency pulsed electromagnetic therapy for acute whiplash injuries. A double blind randomized controlled study. *Scand. J. Rehabil. Med.* **24**, 51–59 (1992).
31. A. Wixforth, Acoustically driven planar microfluidics. *Superlattices Microstruct.* **33**, 389–396 (2003).

32. "Understanding effects of viscosity in the BioFlux system" (Technical Note 1–2, Fluxion, 2009).
33. J. T. Hancock, R. Desikan, S. J. Neill, Role of reactive oxygen species in cell signalling pathways. *Biochem. Soc. Trans.* **29**, 345–350 (2001).
34. R. J. Duronio, Y. Xiong, Signaling pathways that control cell proliferation. *Cold Spring Harb. Perspect. Biol.* **5**, a008904 (2013).
35. C. J. Cattin *et al*., Mechanical control of mitotic progression in single animal cells. *Proc. Natl. Acad. Sci. U.S.A.* **112**, 11258–11263 (2015).
36. S. J. Streichan, C. R. Hoerner, T. Schneidt, D. Holzer, L. Hufnagel, Spatial constraints control cell proliferation in tissues. *Proc. Natl. Acad. Sci. U.S.A.* **111**, 5586–5591 (2014).
37. A. Puliafito *et al*., Collective and single cell behavior in epithelial contact inhibition. *Proc. Natl. Acad. Sci. U.S.A.* **109**, 739–744 (2012).
38. C. Ribeiro *et al*., Enhanced proliferation of pre-osteoblastic cells by dynamic piezoelectric stimulation. *RSC Advances* **2**, 11504–11509 (2012).
39. M. B. Esch *et al*., Multi-cellular 3D human primary liver cell culture elevates metabolic activity under fluidic flow. *Lab Chip* **15**, 2269–2277 (2015).
40. G. Weder *et al*., Measuring cell adhesion forces during the cell cycle by force spectroscopy. *Biointerphases* **4**, 27–34 (2009).
41. M. L. C. Albuquerque, C. M. Waters, U. Savla, H. W. Schnaper, A. S. Flozak, Shear stress enhances human endothelial cell wound closure in vitro. *Am. J. Physiol. Heart Circ. Physiol.* **279**, H293–H302 (2000).
42. J. Bednarz, A. Thalmann-Goetsch, G. Richard, K. Engelmann, Influence of vascular endothelial growth factor on bovine corneal endothelial cells in a wound-healing model. *Ger. J. Ophthalmol.* **5**, 127–131 (1996).
43. B. L. Coomber, Centrosome reorientation in regenerating endothelial monolayers requires bFGF. *J. Cell. Biochem.* **52**, 289–296 (1993).
44. W. H. Reinhart, Shear-dependence of endothelial functions. *Experientia* **50**, 87–93 (1994).
45. C. R. White, J. A. Frangos, The shear stress of it all: The cell membrane and mechanochemical transduction. *Philos. Trans. R. Soc. Lond. B Biol. Sci.* **362**, 1459–1467 (2007).
46. C. F. Dewey, Jr, S. R. Bussolari, M. A. Gimbrone, Jr, P. F. Davies, The dynamic response of vascular endothelial cells to fluid shear stress. *J. Biomech. Eng.* **103**, 177–185 (1981).
47. C. F. Dewey, Jr, Effects of fluid flow on living vascular cells. *J. Biomech. Eng.* **106**, 31–35 (1984).
48. A. Dardik, A. Yamashita, F. Aziz, H. Asada, B. E. Sumpio, Shear stress-stimulated endothelial cells induce smooth muscle cell chemotaxis via platelet-derived growth factor-BB and interleukin-1α. *J. Vasc. Surg.* **41**, 321–331 (2005).
49. S. Hsu, R. Thakar, D. Liepmann, S. Li, Effects of shear stress on endothelial cell haptotaxis on micropatterned surfaces. *Biochem. Biophys. Res. Commun.* **337**, 401–409 (2005).
50. H. Jo *et al*., Differential effect of shear stress on extracellular signal-regulated kinase and N-terminal Jun kinase in endothelial cells. Gi2- and Gbeta/γ-dependent signaling pathways. *J. Biol. Chem.* **272**, 1395–1401 (1997).
51. S. Dimmeler, J. Haendeler, V. Rippmann, M. Nehls, A. M. Zeiher, Shear stress inhibits apoptosis of human endothelial cells. *FEBS Lett.* **399**, 71–74 (1996).
52. M. Chabanon *et al*., Histological method to study the effect of shear stress on cell proliferation and tissue morphology in a bioreactor. *Tissue Eng. Regen. Med.* **16**, 225–235 (2019).
53. U. M. Liegibel *et al*., Fluid shear of low magnitude increases growth and expression of TGFbeta1 and adhesion molecules in human bone cells in vitro. *Exp. Clin. Endocrinol. Diabetes* **112**, 356–363 (2004).
54. V. I. Sikavitsas *et al*., "Fluid flow increases mineralized matrix deposition in three-dimensional perfusion culture of marrow stromal osteoblasts in a dose-dependent manner" in *Annual International Conference of the IEEE Engineering in Medicine and Biology–Proceedings* (Institute of Electrical and Electronics Engineers, New York, 2002), 1, pp. 884–885.
55. P. P. Hsu *et al*., Effects of flow patterns on endothelial cell migration into a zone of mechanical denudation. *Biochem. Biophys. Res. Commun.* **285**, 751–759 (2001).
56. F. Sachs, C. E. Morris, Mechanosensitive ion channels in nonspecialized cells. *Rev. Physiol. Biochem. Pharmacol.* **132**, 1–77 (1998).
57. C. D. Cox, N. Bavi, B. Martinac, Biophysical principles of ion-channel-mediated mechanosensory transduction. *Cell Rep.* **29**, 1–12 (2019).
58. L. L. Demer, C. M. Wortham, E. R. Dirksen, M. J. Sanderson, Mechanical stimulation induces intercellular calcium signaling in bovine aortic endothelial cells. *Am. J. Physiol.* **264**, H2094–H2102 (1993).
59. R. V. Sharma *et al*., Mechanical stimulation increases intracellular calcium concentration in nodose sensory neurons. *Neuroscience* **66**, 433–441 (1995).
60. M. J. Ryan, K. W. Gross, G. Hajduczok, Calcium-dependent activation of phospholipase C by mechanical distension in renin-expressing As4.1 cells. *Am. J. Physiol. Endocrinol. Metab.* **279**, E823–E829 (2000).
61. E. J. Pettit, F. S. Fay, Cytosolic free calcium and the cytoskeleton in the control of leukocyte chemotaxis. *Physiol. Rev.* **78**, 949–967 (1998).
62. R. A. Brundage, K. E. Fogarty, R. A. Tuft, F. S. Fay, Calcium gradients underlying polarization and chemotaxis of eosinophils. *Science* **254**, 703–706 (1991).
63. D. E. Clapham, Calcium signaling. *Cell* **131**, 1047–1058 (2007).
64. N. Prevarskaya, R. Skryma, Y. Shuba, Calcium in tumour metastasis: New roles for known actors. *Nat. Rev. Cancer* **11**, 609–618 (2011).
65. A. K. Howe, Cross-talk between calcium and protein kinase A in the regulation of cell migration. *Curr. Opin. Cell Biol.* **23**, 554–561 (2011).
66. N. Wang, D. E. Ingber, Control of cytoskeletal mechanics by extracellular matrix, cell shape, and mechanical tension. *Biophys. J.* **66**, 2181–2189 (1994).
67. N. Wang, J. Butler, D. Ingber, Mechanotransduction across the cell surface and through the cytoskeleton. *Science* **260**, 1124–1127 (1993).
68. B. D. Matthews, D. R. Overby, R. Mannix, D. E. Ingber, Cellular adaptation to mechanical stress: Role of integrins, Rho, cytoskeletal tension and mechanosensitive ion channels. *J. Cell Sci.* **119**, 508–518 (2006).
69. A. M. Jötten *et al*., Correlation of in vitro cell adhesion, local shear flow and cell density. *RSC Advances* **9**, 543–551 (2019).
70. M. Voss *et al*., Shedding of glycan-modifying enzymes by signal peptide peptidase-like 3 (SPPL3) regulates cellular N-glycosylation. *EMBO J.* **33**, 2890–2905 (2014).
71. P.-H. Kuhn *et al*., Secretome analysis identifies novel signal peptide peptidase-like 3 (Sppl3) substrates and reveals a role of Sppl3 in multiple Golgi glycosylation pathways. *Mol. Cell. Proteomics* **14**, 1584–1598 (2015).
72. E. K. Paluch *et al*., Mechanotransduction: Use the force(s). *BMC Biol.* **13**, 47 (2015).
73. H. Jin *et al*., Flexible surface acoustic wave resonators built on disposable plastic film for electronics and lab-on-a-chip applications. *Sci. Rep.* **3**, 2140 (2013).
74. K. Beck *et al*., Inductively coupled surface acoustic wave device for sensor application. *IEEE Trans. Ultrason. Ferroelectr. Freq. Control* **45**, 1140–1144 (1998).